CHAPTER IV

THE PROPOSED SWITCHING FLOW-GRAPH MODELING TECHNIQUE FOR THREE-PHASE RECTIFIERS

4.1 The Concept of Virtual Switch

The virtual switches for the three-phase rectifier can be found by the same procedures as illustrated in section III. Consider a typical three-phase PWM rectifier as shown in Fig. 4.1 where S_{jP}, S_{jN} and D_{jP}, D_{jN}, $j \in \{A,B,C\}$ represent controllable switches and diodes respectively and a RC impedance load is connected as an example. In order to properly control the switches of the rectifier, two constraints should be met at any time. 1) Switch S_{jP} and S_{jN}, $j \in \{A,B,C\}$ should not be ON simultaneously to avoid short circuit. 2) It is not allowed to result in an open circuit for any phase. There are sixteen switching states for each phase according to the combination of ON/OFF states of each switch and each diode. Nevertheless, only six switching states as described in Table 4.1 are qualified for the rectifier operation.

Table 4.1 Six qualified switching states

Value of v_{jN}	*State Number*	*Switching States* $(S_{jP}, D_{jP}, S_{jN}, D_{jN})$
$v_{jN} = V_{DC}$	*State 1*	*(OFF, ON, OFF, OFF)*
	State 2	*(ON, OFF, OFF, OFF)*
	State 3	*(ON, ON, OFF, OFF)*
$v_{jN} = 0$	*State 4*	*(OFF, OFF, OFF, ON)*
	State 5	*(OFF, OFF, ON, OFF)*
	State 6	*(OFF, OFF, ON, ON)*

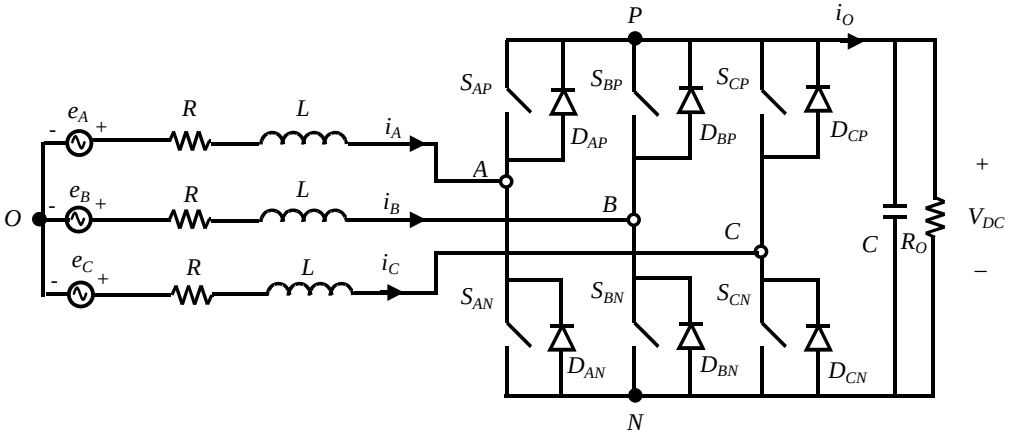

Fig. 4.1 The circuit configuration of the PWM rectifier

From Table 4.1, one can see that for j-phase $j \in \{A,B,C\}$, states 2, 4 and 6 only occur for $i_j < 0$ and states 1, 3, and 5 occur for $i_j > 0$. Also, the value of v_{jN} equals to V_{DC} for states 1, 2 and 3 and zero for states 4, 5, and 6. Similar to [32], for the controllable switches of Fig. 1 one can define the basic switching functions:

$$F_{S_{jk}}(t) = \begin{cases} 1, & \text{when } S_{jk} \text{ is } ON \\ 0, & \text{when } S_{jk} \text{ is } OFF \end{cases} \tag{4.1}$$

$$\overline{F_{S_{jk}}}(t) = \begin{cases} 1, & \text{when } S_{jk} \text{ is } OFF \\ 0, & \text{when } S_{jk} \text{ is } ON \end{cases} \tag{4.2}$$

$$j \in \{A,B,C\}, \quad k \in \{P,N\}$$

In order to deal with the different voltage polarities, the operation conditions of diodes are described clearly as following.

If $\left[\left(S_{jN} \text{ is } OFF\right) \text{ AND } \left(i_j(t) > 0\right)\right]$ *is true, then* D_{jP} *is ON; otherwise,* D_{jP} *is OFF.*

If $\left[\left(S_{jP} \text{ is } OFF\right) \text{ AND } \left(i_j(t) < 0\right)\right]$ *is true, then* D_{jN} *is ON; otherwise,* D_{jN} *is OFF.*

$j \in \{A,B,C\}$

Therefore, the switching functions of diodes can be defined as:

$$F_{D_{jP}}(t) \overset{\Delta}{=} \begin{cases} 1, & when \ \ D_{jP} \ \ is \ \ ON \\ 0, & when \ \ D_{jP} \ \ is \ \ OFF \end{cases} = \overline{F_{S_{jN}}}(t) \ \ AND \ \ \left(sign(i_j)\right) \tag{4.3}$$

$$F_{D_{jN}}(t) \overset{\Delta}{=} \begin{cases} 1, & when \ \ D_{jN} \ \ is \ \ ON \\ 0, & when \ \ D_{jN} \ \ is \ \ OFF \end{cases} = \overline{F_{S_{jP}}}(t) \ \ AND \ \ \left(sign(-i_j)\right) \tag{4.4}$$

$$sign(x) \overset{\Delta}{=} \begin{cases} 1, & x > 0 \\ 0, & x < 0 \end{cases} \tag{4.5}$$

$$j \in \{A, B, C\}$$

Thus, based on the previous definitions one can now define the virtual switch S_j for leg-j in Fig. 4.1 with the following operation condition:

$$If \ \ \{ \ [(S_{jP} \ \ is \ \ ON) \ \ AND \ \ (i_j < 0)] \ \ OR \ \ (D_{jP} \ \ is \ \ ON) \ \}$$
$$is \ \ true, \ then \ \ S_j \ \ is \ \ ON; \ otherwise, \ \ S_j \ \ is \ \ OFF.$$
$$j \in \{A, B, C\}$$

Also, the corresponding virtual switching functions $F_j(t)$ and $\overline{F_j}(t)$ of S_j are defined as:

$$F_j(t) \overset{\Delta}{=} \begin{cases} 1, & when \ \ S_j \ \ is \ \ ON \\ 0, & when \ \ S_j \ \ is \ \ OFF \end{cases} = \left[F_{S_{jP}}(t) \ \ AND \ \ sign(-i_j)\right] \ \ OR \ \ F_{D_{jP}}(t) \tag{4.6}$$

$$\overline{F_j}(t) \overset{\Delta}{=} \begin{cases} 1, & when \ \ S_j \ \ is \ \ OFF \\ 0, & when \ \ S_j \ \ is \ \ ON \end{cases} = \left[F_{S_{jN}}(t) \ \ AND \ \ sign(i_j)\right] \ \ OR \ \ F_{D_{jN}}(t) \tag{4.7}$$

$$F_j(t) + \overline{F_j}(t) = 1$$
$$j \in \{A, B, C\} \tag{4.8}$$

From the definition of the virtual switches and the virtual switching functions, one can easily obtain the equivalent circuit as shown in Fig. 4.2. For easy understanding, Fig. 4.3 also shows the corresponding virtual switching function.

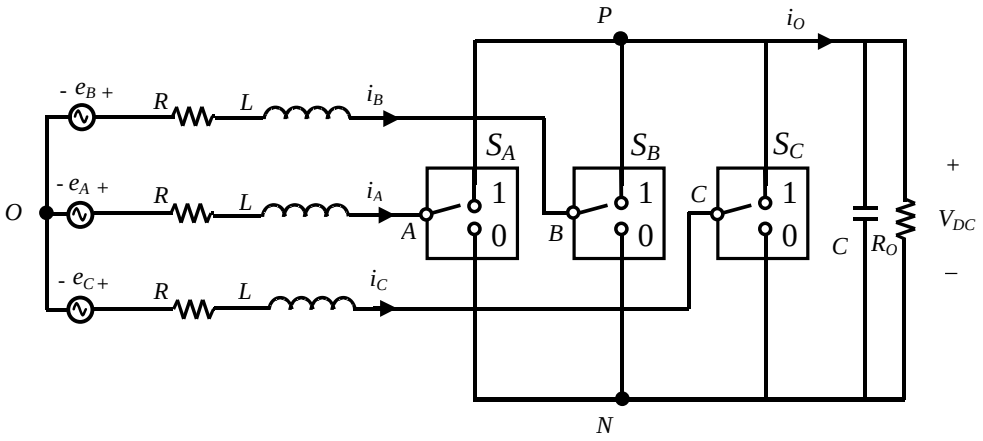

Fig. 4.2 Equivalent circuit of Fig. 4.1

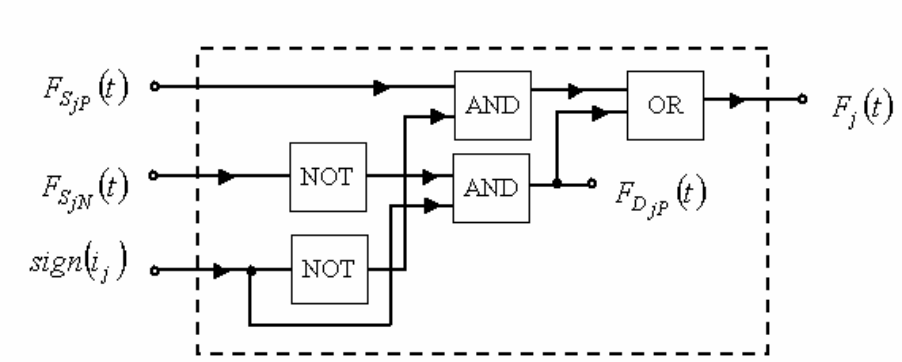

Fig. 4.3 The corresponding virtual switching function.

According to Fig. 4.2, the voltage equations and current equation can be written as:

$$v_{jN}(t) = V_{DC} F_j(t) \tag{4.9}$$

$$e_j(t) = R i_j(t) + L\frac{di_j(t)}{dt} + F_j(t) V_{DC} + v_{NO} \tag{4.10}$$

$$i_O(t) = \sum_j F_j(t) i_j(t) \tag{4.11}$$

$$j \in \{A, B, C\}$$

From the condition $i_A + i_B + i_C = 0$, one can get

$$v_{NO} = -\tfrac{1}{3}\left(F_A(t) + F_B(t) + F_C(t)\right) V_{DC} \tag{4.12}$$

Substitute equation (4.12) into equation (4.10), the voltage equation can be rewritten as:

$$e_A = Ri_A + L\frac{di_A}{dt} + \left(\tfrac{2}{3}F_A - \tfrac{1}{3}F_B - \tfrac{1}{3}F_C\right)V_{DC} \quad (4.13a)$$

$$e_B = Ri_B + L\frac{di_B}{dt} + \left(\tfrac{2}{3}F_B - \tfrac{1}{3}F_A - \tfrac{1}{3}F_C\right)V_{DC} \quad (4.13b)$$

$$e_C = Ri_C + L\frac{di_C}{dt} + \left(\tfrac{2}{3}F_C - \tfrac{1}{3}F_B - \tfrac{1}{3}F_A\right)V_{DC} \quad (4.13c)$$

According to equations (4.11) and (4.13), the proposed switching flow-graph for three-phase PWM rectifier can be drawn as Fig. 4.4.

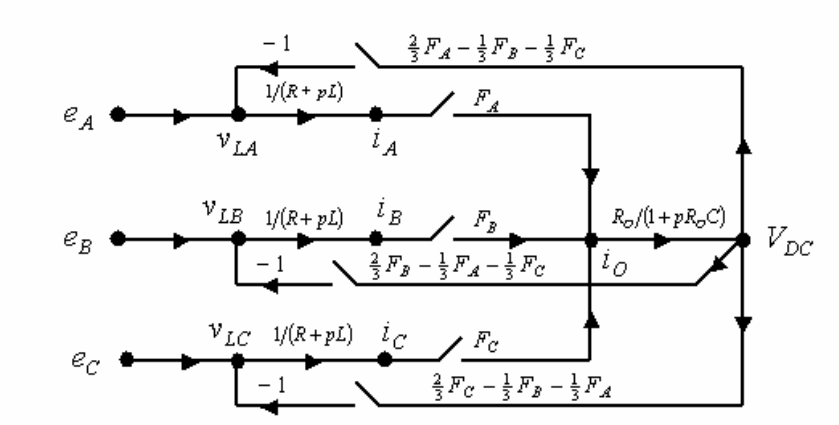

Fig. 4.4 The proposed switching flow-graph model for three-phase PWM rectifier.

4.2 The Proposed Switching Flow-Graph Model for Thee-Phase Rectifiers

From the definitions of the switching functions, one can observe that as the switching function equals to one, the input signal of the switching branch will pass through the branch. Otherwise, as the switching function equals to zero, the input signal of the switching branch will be intercepted and cut off. The switching branch can be regarded as a gate that controlled by the switching functions. The condition is similar when the virtual switching functions are carried on the switching branch; the input signal of the switching branches can pass or not, is determined by the virtual switching functions. Therefore, the large-signal model, as shown in Fig. 4.5, can be obtained directly by replacing the switching branches of Fig. 4.4 with multipliers.

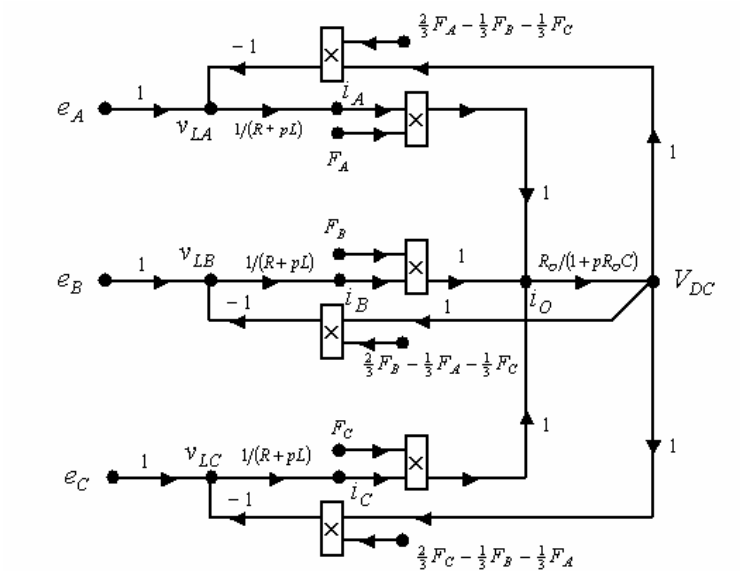

Fig. 4.5 The large-signal model derived from Fig. 4.4.

When the ON-resistanc R_{ON} of switches is considered, another virtual switching functions F_{jR}, $j \in \{A,B,C\}$, as equation (4.14), can be defined to describe the effect caused by ON-resistance R_{ON}.

$$F_{jR}(t) = F_{S_{jP}}(t) \quad OR \quad F_{S_{jN}}(t) \qquad (4.14)$$
$$j \in \{A,B,C\}$$

The resulting large-signal switching flow-graph is shown in Fig. 4.6

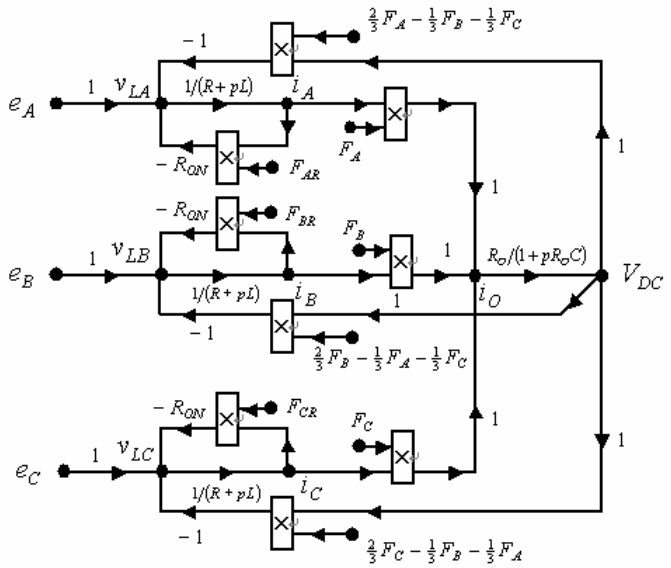

Fig. 4.6 The large-signal switching flow-graph model considering ON-resistance of active switches.

4.3 The Corresponding Models Derived from Switching Flow-Graph Model

A. Large-Signal Model

When the switching frequency is high, the corresponding duty ratio of the virtual switching function can be obtained by averaging the virtual switching function over a switching period, as described in equation (4.15).

$$d_j(t) \overset{\Delta}{=} \frac{1}{T_S}\int_{t}^{t+T_S} F_j(\lambda)d\lambda \qquad (4.15)$$
$$j \in \{A, B, C\}$$

According to the state space averaging technique, the characteristic equations of the three-phase PWM rectifier (equations (4.11) and (4.13)) can be re-written by replacing the virtual switching functions with the corresponding duty ratios, as described bellow:

$$C\frac{dV_{DC}}{dt} = \sum_j d_j(t) i_j(t) - \frac{V_{DC}}{R_O} \qquad (4.16)$$
$$j \in \{A, B, C\}$$
$$e_A = (R + pL)i_A + \left(\tfrac{2}{3}d_A - \tfrac{1}{3}d_B - \tfrac{1}{3}d_C\right)V_{DC} \qquad (4.17a)$$
$$e_B = (R + pL)i_B + \left(\tfrac{2}{3}d_B - \tfrac{1}{3}d_A - \tfrac{1}{3}d_C\right)V_{DC} \qquad (4.17b)$$
$$e_C = (R + pL)i_C + \left(\tfrac{2}{3}d_C - \tfrac{1}{3}d_B - \tfrac{1}{3}d_A\right)V_{DC} \qquad (4.17c)$$

Then, by taking the conventional d-q transformation, the characteristic equations in synchronous reference frame can be described as equations (4.18) - (4.20).

$$e_d = L\frac{di_d}{dt} + Ri_d - \omega L i_q + d_d V_{DC} \qquad (4.18)$$
$$e_q = L\frac{di_q}{dt} + Ri_q + \omega L i_d + d_q V_{DC} \qquad (4.19)$$
$$C\frac{dV_{DC}}{dt} + \frac{V_{DC}}{R_O} = i_d d_d + i_q d_q \qquad (4.20)$$

According to equations (4.18) – (4.20), one can develop a signal flow-graph, as shown in Fig. 4.7, to describe the relationship between the variables; where ω is the angular frequency (rad/s).

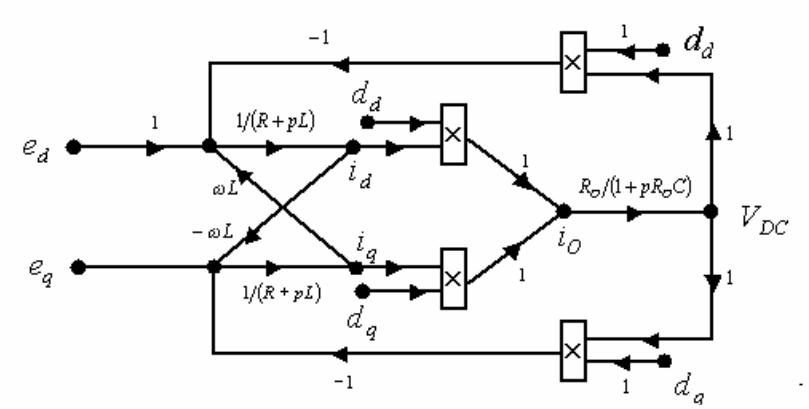

Fig. 4.7 The large-signal model of the three-phase rectifier based on d-q coordinate.

B. Steady State Model

As the system approaches to steady state, the variables will keep constant and the differential items will be zero. Therefore, from equations (4.18) – (4.20), the steady state relation can be expressed as:

$$E_d = RI_d - \omega LI_q + D_d V_{DC} \tag{4.21}$$

$$E_q = RI_q + \omega LI_d + D_q V_{DC} \tag{4.22}$$

$$\frac{V_{DC}}{R_O} = I_d D_d + I_q D_q \tag{4.23}$$

The steady state signal of e_d, e_q, i_d, i_q, d_d, and d_q are represented as E_d, E_q, I_d, I_q, D_d, and D_q, respectively. Therefore, according to equations (4.21) – (4.23), the steady-state model can be easily developed in flow-graph form as depicted in Fig. 4.8.

C. Small-Signal Model

According to reference [32], one can easily obtain the small-signal model from the signal-flow graph shown in Fig. 4.7. As explained in Fig. 4.9a, if two variables, d and x, are multiplied together in the large-signal model, the small-signal relation of the two variables is equal to $\hat{d}X + \hat{x}D$ by ignoring the second order items; where $\hat{d}$, $\hat{x}$ and D, X mean the small perturbations and the steady state signal of d

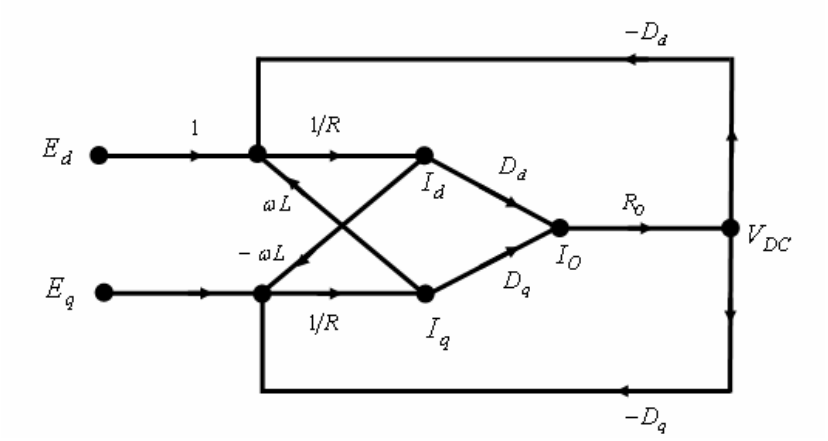

Fig. 4.8 The steady state model based on d-q coordinate.

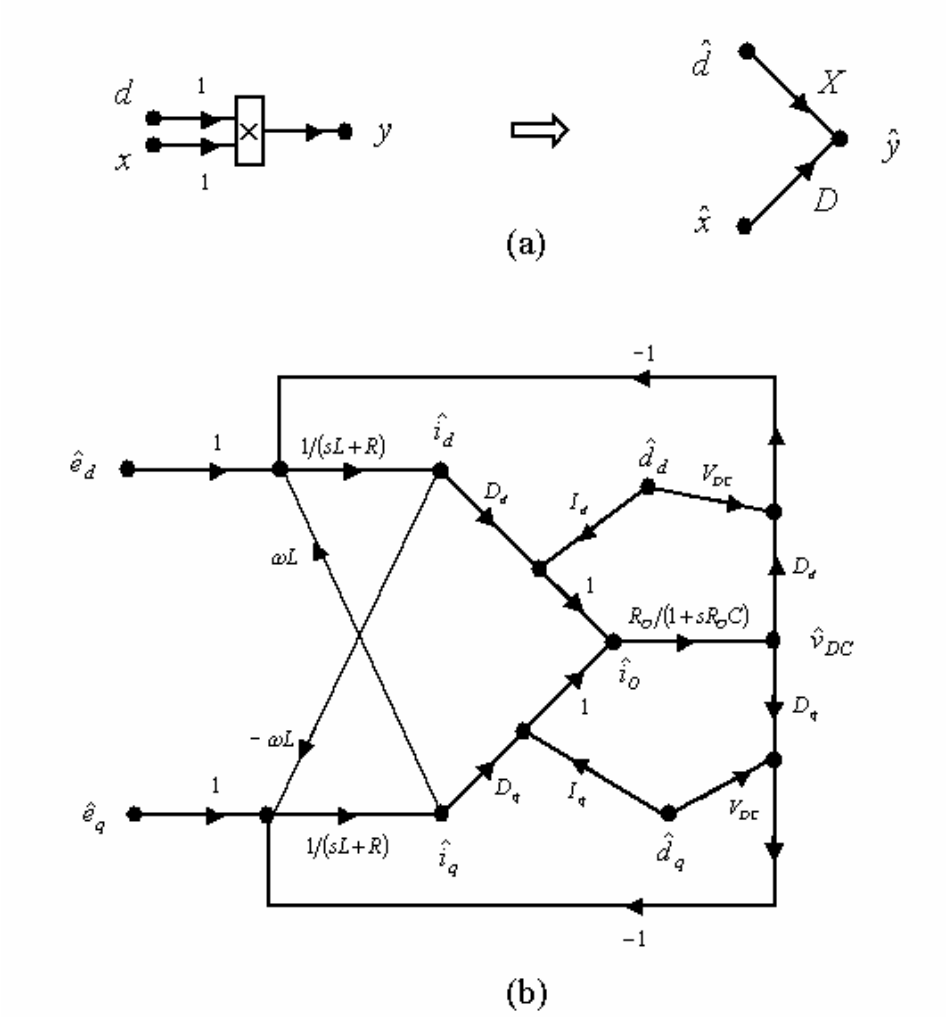

Fig. 4.9 (a) The small-signal expression for two variables multiplied together, (b) the small-signal model based on d-q coordinate.

and x respectively. Therefore, by modifying from Fig. 4.7, the small-signal model, shown in Fig. 4.9b can straightforwardly be developed. The small perturbations of e_d, e_q, i_d, i_q, d_d, d_q and v_{DC} are represented as $\hat{e}_d$, $\hat{e}_q$, $\hat{i}_d$, $\hat{i}_q$, $\hat{d}_d$, $\hat{d}_q$, and $\hat{v}_{DC}$ respectively. The steady state signals of v_{DC}, i_d, i_q, d_d, and d_q are expressed as V_{DC}, I_d, I_q, D_d, and D_q respectively.

By reason of the symmetric structure of the small-signal model, the transfer functions are simple to derive by using Mason's rule. The transfer functions $\hat{v}_O(s)/\hat{d}_d(s)$, $\hat{v}_O(s)/\hat{d}_q(s)$, $\hat{v}_O(s)/\hat{e}_d(s)$ and $\hat{v}_O(s)/\hat{e}_q(s)$ are listed in the following:

$$\frac{\hat{v}_{DC}(s)}{\hat{d}_d(s)} = \frac{M_{1d}(1-\Delta_1)+M_{2d}+M_{3d}}{1-\sum_{j=1}^{5}\Delta_j} \tag{4.24}$$

$$\frac{\hat{v}_{DC}(s)}{\hat{d}_q(s)} = \frac{M_{1q}(1-\Delta_1)+M_{2q}+M_{3q}}{1-\sum_{j=1}^{5}\Delta_j} \tag{4.25}$$

$$\frac{\hat{v}_{DC}(s)}{\hat{e}_d(s)} = \frac{N_{1d}+N_{2d}}{1-\sum_{j=1}^{5}\Delta_j} \tag{4.26}$$

$$\frac{\hat{v}_{DC}(s)}{\hat{e}_d(s)} = \frac{N_{1q}+N_{2q}}{1-\sum_{j=1}^{5}\Delta_j} \tag{4.27}$$

$$M_{1d} = I_d \frac{R_O}{sCR_O+1} \qquad M_{1d} = I_q \frac{R_O}{sCR_O+1}$$

$$M_{2d} = -V_{DC}D_d \frac{1}{(sL+1)}\frac{R_O}{(sCR_O+1)} \qquad M_{2d} = -V_{DC}D_q \frac{1}{(sL+1)}\frac{R_O}{(sCR_O+1)}$$

$$M_{3d} = V_{DC}\omega LD_q \frac{1}{(sL+1)^2}\frac{R_O}{(sCR_O+1)} \qquad M_{3d} = -V_{DC}\omega LD_d \frac{1}{(sL+1)^2}\frac{R_O}{(sCR_O+1)}$$

$$N_{1d} = D_d \frac{1}{(sL+1)}\frac{R_O}{(sCR_O+1)} \qquad N_{1q} = D_q \frac{1}{(sL+1)}\frac{R_O}{(sCR_O+1)}$$

$$N_{2d} = -\omega LD_q \frac{1}{(sL+1)^2}\frac{R_O}{(sCR_O+1)} \qquad N_{2q} = \omega LD_d \frac{1}{(sL+1)^2}\frac{R_O}{(sCR_O+1)}$$

$$\Delta_1 = -(\omega L)^2 \frac{1}{(sL+1)^2}$$

$$\Delta_2 = -{D_d}^2 \frac{1}{(sL+1)} \frac{R_O}{(sCR_O+1)}$$

$$\Delta_3 = D_d \omega L D_q \frac{1}{(sL+1)^2} \frac{R_O}{(sCR_O+1)}$$

$$\Delta_4 = -{D_q}^2 \frac{1}{(sL+1)} \frac{R_O}{(sCR_O+1)}$$

$$\Delta_5 = -D_q \omega L D_d \frac{1}{(sL+1)^2} \frac{R_O}{(sCR_O+1)}$$

The transfer functions from arbitrary state variable to another arbitrary state variable can easily be obtained by using the same method.

4.4 Simulation Results

From previous results one can see that the structure of the resulting SFG model is very similar to the simulation structure of MATLAB/SIMULINK. Hence, it is quite easy to implement the model in SIMULINK environment to get the simulation results without requiring other extra efforts. As illustrations, some examples are given below.

Consider the example as shown in Fig. 4.1 where $R_O = 160\Omega$, $C = 190\mu F$, $R = 0.3\Omega$ and $L = 10mH$. The AC sources are set to be:

$$e_A(t) = 110\sin(120\pi t)$$
$$e_B(t) = 110\sin(120\pi t - 120^\circ)$$
$$e_C(t) = 110\sin(120\pi t + 120^\circ)$$

Assume the well known sinusoidal PWM is adopted with switching frequency $f_S = 1kHz$ and the amplitude of the triangular wave is $5V$. Also, the voltage command signals are given as follows:

$$V_{control\_A}(t) = 3\sin(120\pi t)$$
$$V_{control\_B}(t) = 3\sin(120\pi t - 120^\circ)$$
$$V_{control\_C}(t) = 3\sin(120\pi t + 120^\circ)$$

A. $R_{ON} = 0.23\Omega$ and $Blanking - time = 0\,\text{sec}$

The ON-resistance of 0.23Ω for each active switch is according to the SPICE model of IRFP460 from PSPICE library. Fig. 4.10 and Fig. 4.11 show the waveforms of output voltage and AC current, respectively. The simulation results shown in Figs. 10(a) and 11(a) are generated from the proposed SFG model. For comparison, the same example is carried out by using PSPICE and under the same conditions. The corresponding results are described in Fig. 10(b) and 11(b). One can see that the simulation results of the proposed SFG model are well confirmed with the results generated from PSPICE. However, the computation time required by using the proposed switching flow-graph model is much less than that required by using PSPICE. When running a PC with Intel Pentium 4 1.6G CPU/ 512MB RAM and with $10\mu s$ step size, it takes only *3* seconds by using the proposed model as compared with *25* seconds by using PSPICE program for *100ms* simulation time period.

B. $R_{ON} = 0.23\Omega$ and $Blanking - time = 40\mu\,\text{sec}$

Fig. 4.12 shows the waveforms of switching functions $F_{S_{AP}}(t)$ and $F_{S_{AN}}(t)$, $F_{D_{AP}}(t)$ and, $F_{D_{AN}}(t)$ and virtual switching function $F_A(t)$. The simulation results indeed agree with the results from virtual switching functions as described in equations (4.3) - (4.8).

The simulation results of output voltage and AC current are depicted in Fig. 4.13 and Fig. 4.14, respectively. One can find that the prediction from the proposed SFG model is well confirmed with the results generated from PSPICE.

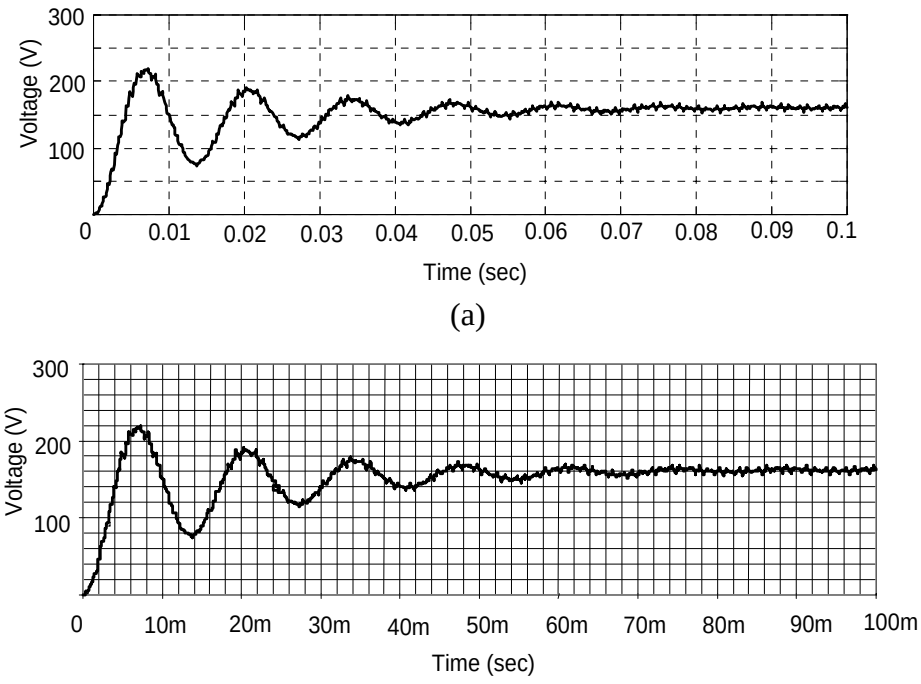

Fig. 4.10 The Simulation results of the output voltage using (a) proposed SFG model, (b) PSPICE model.

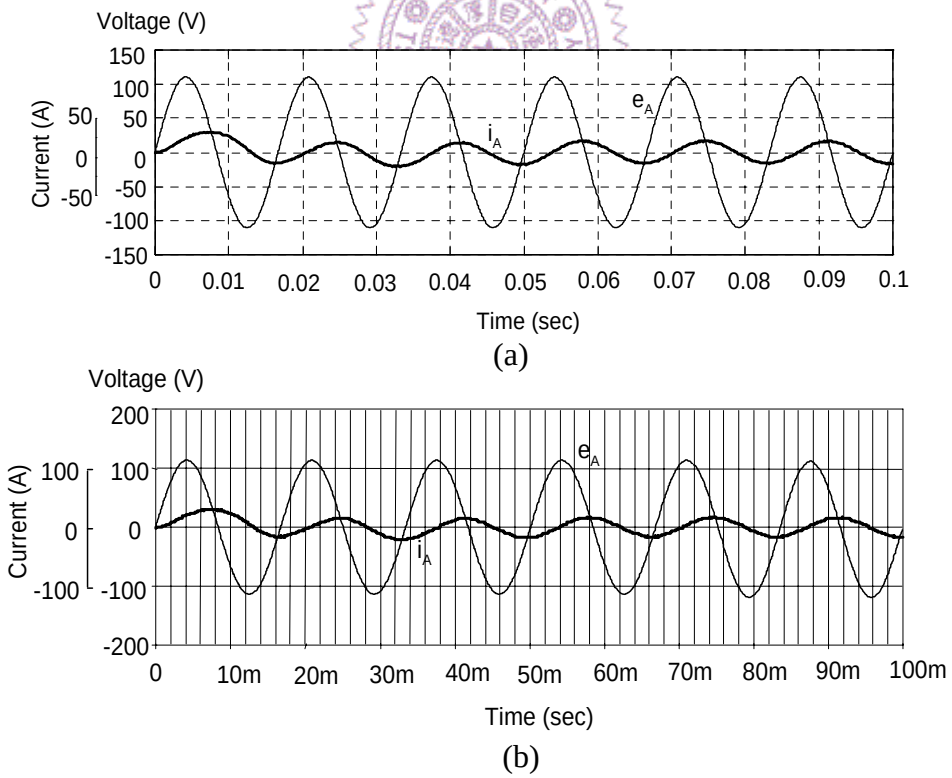

Fig. 4.11 The Simulation results of the AC current and voltage for A-phase using (a) proposed SFG model, (b) PSPICE model.

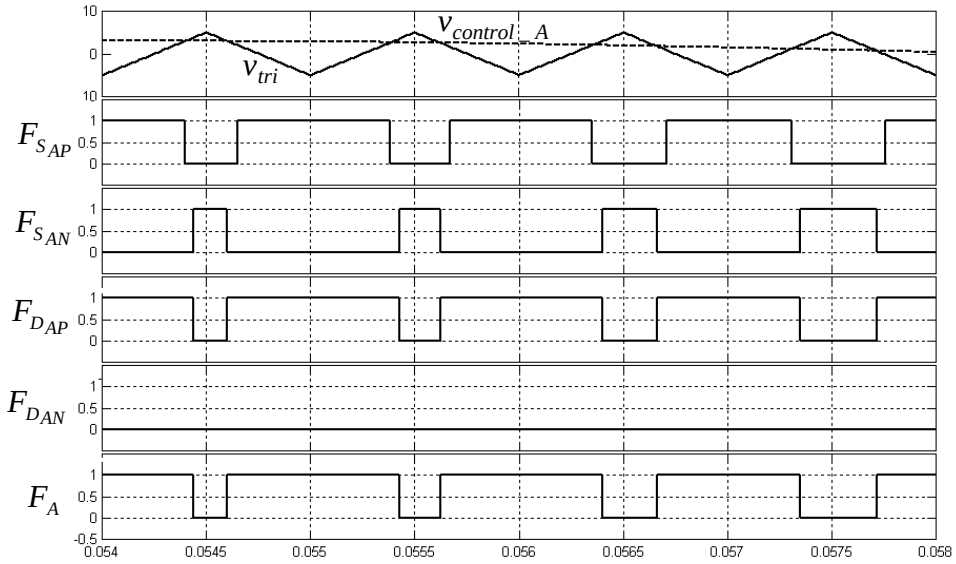

(a)

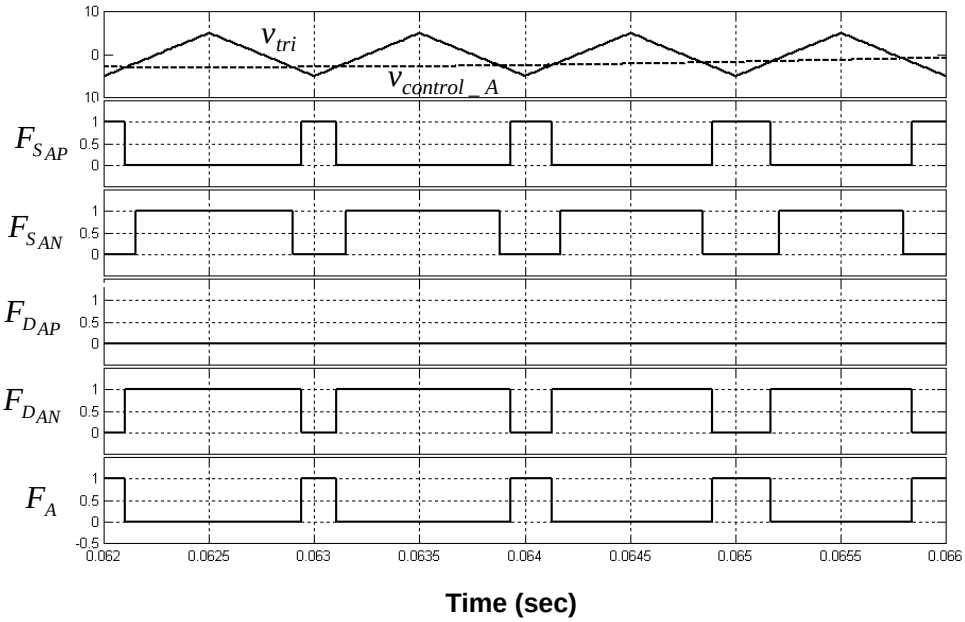

(b)

Fig. 4.12 Waveforms of $F_{S_{AP}}$, $F_{S_{AN}}$, $F_{D_{AP}}$, $F_{D_{AN}}$, and F_A for (a) $i_A > 0$, (b) $i_A < 0$.

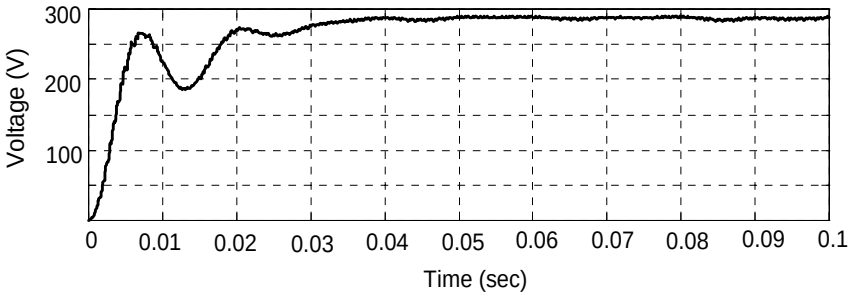

(a)

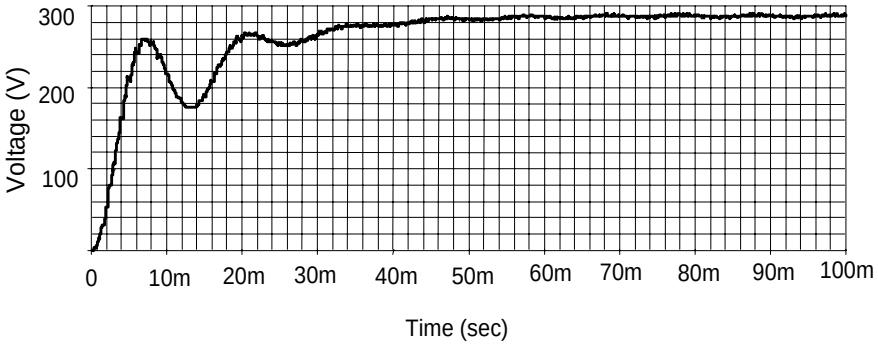

(b)

Fig. 4.13 The Simulation results of the output voltage using (a) proposed SFG model, (b) PSPICE model.

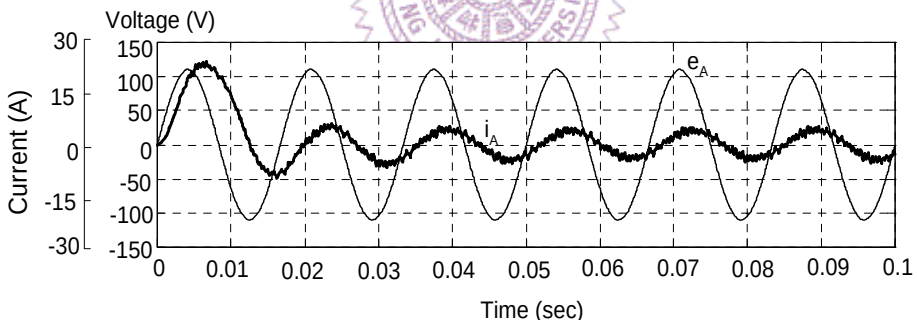

(a)

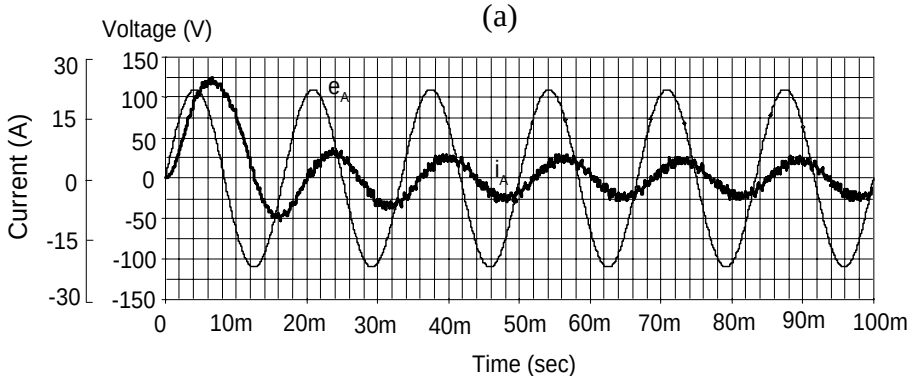

(b)

Fig. 4.14 The Simulation results of the AC current and voltage of A-phase using (a) proposed SFG model, (b) PSPICE model.

C. Experimental Results

Fig. 4.15 shows the DSP-base control system implemented in the lab. Consider the example as shown in Fig. 4.1 where $R_O = 110\Omega$, $C = 2200\mu F$, $R_{ON} = 0.23\Omega$, $R = 0.12\Omega$ and $L = 3.5mH$. The AC sources are set to be:

$$e_A(t) = 50\cos(120\pi t)$$
$$e_B(t) = 50\cos(120\pi t - 120^\circ)$$
$$e_C(t) = 50\cos(120\pi t + 120^\circ)$$

Assume the well known sinusoidal PWM is adopted. The switching frequency of the rectifier is $f_S = 20kHz$ and the amplitude of the triangular wave is $1V$. The rated power of the system is $750W$. Fig. 4.16 shows the simulation and experimental results without controllers when setting $D^*_d = 0.7348$ and $D^*_q = 0$. One can observe that the simulation results closely agree with the experimental results.

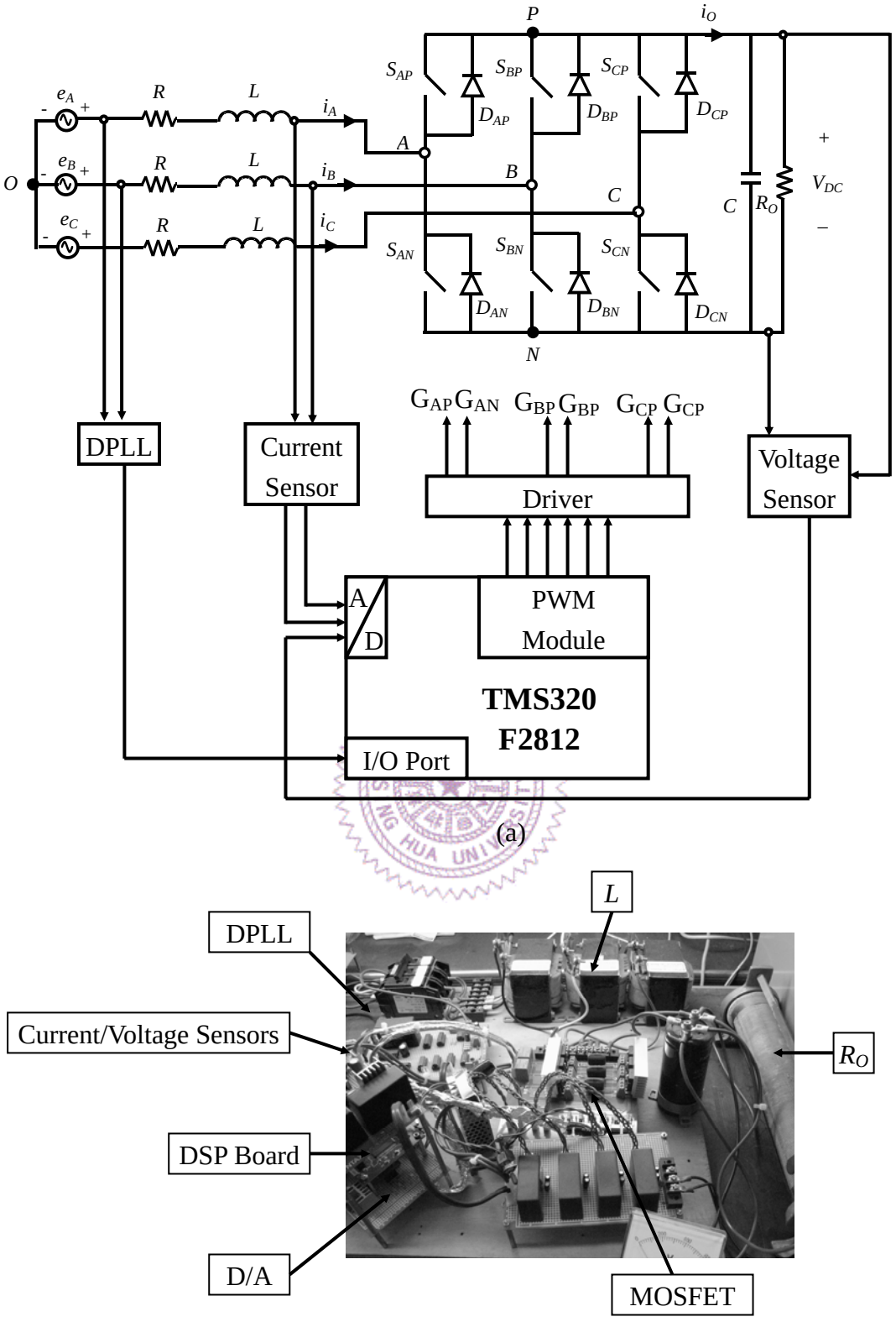

(a)

(b)

Fig. 4.15 (a) The diagram of the experiment, (b)the prototype of the experiment.

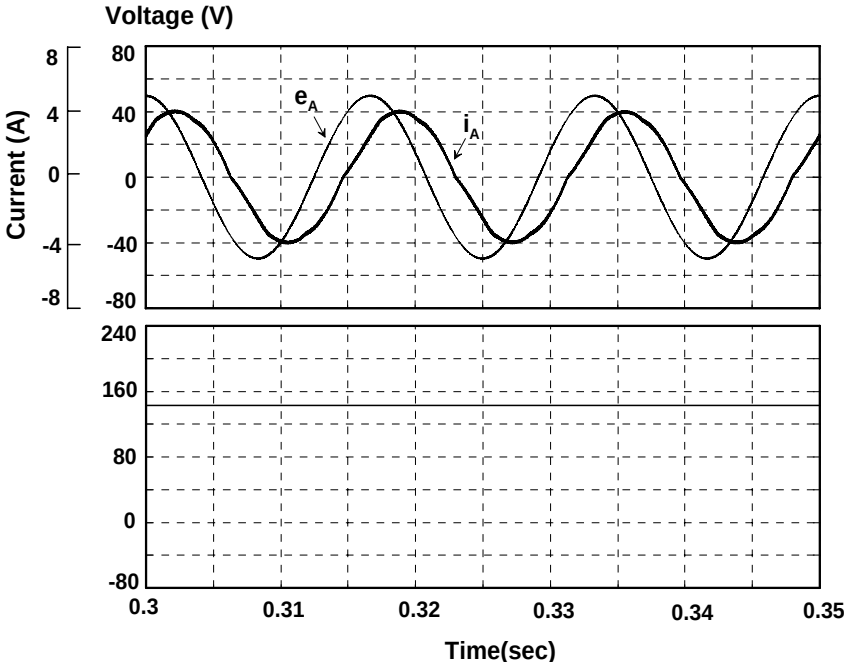

(a)

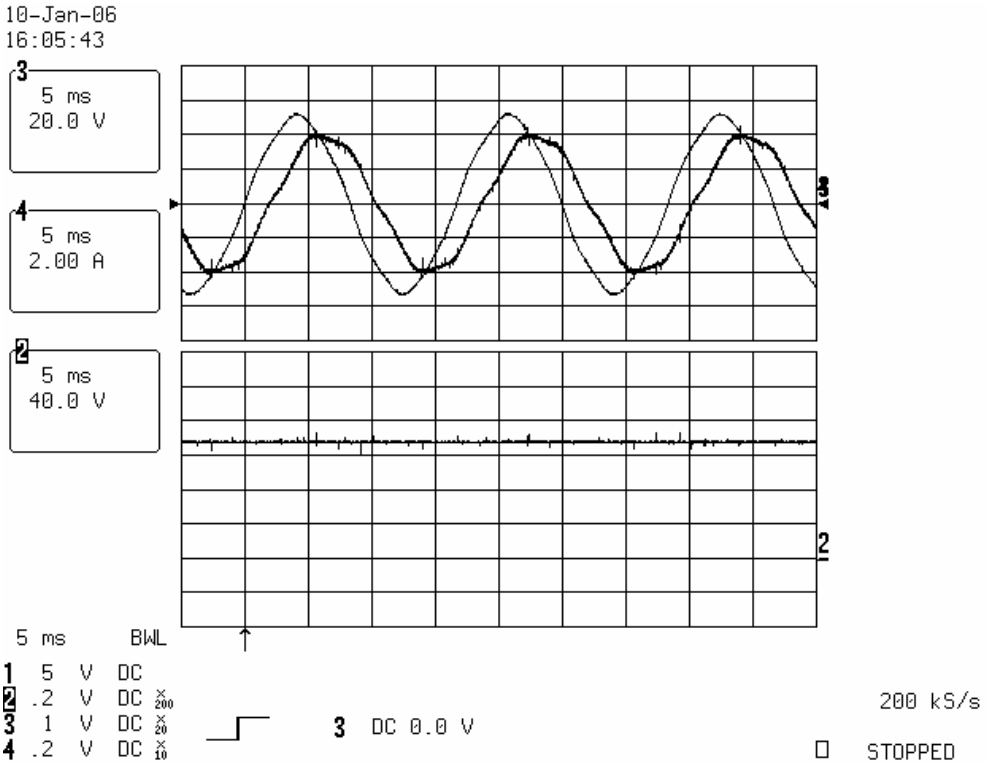

(b)

Fig. 4.16 (a) The simulation waveforms, (b) the experimental waveforms of the phase voltage and current for A-phase without controllers.